Lateral black phosphorene P–N junctions formed via chemical doping for high performance near-infrared photodetector

Zhang, Shengli; Zeng, Haibo; Wang, Qi Jie; Yu, Xuechao

2016

Yu, X., Zhang, S., Zeng, H., & Wang, Q. J. (2016). Lateral black phosphorene P–N junctions formed via chemical doping for high performance near-infrared photodetector. Nano Energy, 25, 34-41.

https://hdl.handle.net/10356/80381

https://doi.org/10.1016/j.nanoen.2016.04.030

Communication

Lateral Black Phosphorene P-N Junctions Formed via Chemical Doping for High Performance Near-infrared Photodetector

Xuechao Yu[a], Shengli Zhang[b], Haibo Zeng[b,*], and Qi Jie Wang[a,*]

[a]Centre for OptoElectronics and Biophotonics, School of Electrical and Electronic Engineering, Nanyang Technological University, 50 Nanyang Avenue, 639798, Singapore

[b]Country Institute of Optoelectronics & Nanomaterials, Herbert Gleiter Institute of Nanoscience, College of Materials Science and Engineering, Nanjing University of Science and Technology, Nanjing, 210094, China

Corresponding email: zeng.haibo@njust.edu.cn (Prof. Haibo Zeng) qjwang@ntu.edu.sg (Prof. Qi Jie Wang)

Abstract

Black phosphorene (BP), a newly discovered elemental two-dimensional material, is attractive for optoelectronic and photonic applications because of its unique in-plane anisotropy, thickness-dependent direct bandgap and high carrier mobility. Since its discovery, black phosphorene has become an appealing candidate well-suited for polarization-resolved near- and mid-infrared optoelectronics due to its relative narrow bandgap and asymmetric structure. Here, we employ benzyl viologen (BV) as an effective electron dopant to part of the area of a p-type few-layer BP flake and achieve an ambient stable, in-plane P-N junction. Chemical doping with BV molecules modulates the electron density and allows acquiring a large built-in potential in this in-plane BP P-N junction, which is crucial for achieving high responsivity photodetectors and high quantum efficiency solar cells. As a demonstrative example, by illuminating it with a near-infrared laser at 1.47 μm, we observe a high responsivity up to ~180 mA/W with a rise time of 15 ms, and an external quantum efficiency of 0.75%. Our strategy for

creating environmentally stable BP P-N junction paves the way to implementing high performance BP phototransistors and solar cells, which is also applicable to other 2D materials.

Keywords: Few-layer black phosphorene; chemical doping; P-N junction; photodetector; solar cells.

1. Introduction

Two-dimensional (2D) crystals have emerged as a novel class of materials with a wide range of remarkable electronic and optoelectronic properties **[1]**. For example, graphene and transition metal dichalcogenides (TDMCs) have rapidly established themselves as intriguing building blocks for photonic and optoelectronic applicationsin such as photodetection **[2, 3]**. Graphene-based photodetectors exhibit broadband and ultrafast photoresponses, however suffering from the low absorption and short photogenerated carrier lifetime due to the gapless nature. **[4]** Consequently, significant efforts have been devoted to exploring photosensitive TMDCs such as single layer MoS_2, a widely investigated 2D semiconductor with a direct bandgap and strong absorption coefficient **[5, 6]**. One of the enduring challenges in MoS_2 photodetectors is the large band gap that limits its operation only in the visible and ultraviolet ranges **[7]**. As a result, novel 2D materials with a direct, small band-gap together with high mobility have been the long pursuit for extending high-performance photodetector in the infrared range.

Very recently, black phosphorene, the most stable allotrope of element phosphorus with strong anisotropy and a direct bandgap ranging from 0.3 eV to 2 eV **[8, 9]** depending on the number of layers, has been isolated by both mechanical cleavage strategy and chemical methods, which was demonstrated to exhibit a mobility up to 1000

$cm^2/V\ s$ **[10-12]**. Fast and broadband photoresponse in the visible and near infrared ranges of few layer black phosphorene has been achieved, filling the gap between zero bandgap graphene and large bandgap TDMC **[13-15]**. However, the performance is limited by the low light absorption and photogenerated carrier separation efficiency. In previous reports, a photovoltaic P-N junction photodetector with high responsivity and detectivity has been realized by applying separate gates to form electrostatically induced P-N junction in other 2D materials **[16]**. The photogenerated electron/hole pairs can be separated by the internal electric field via a photovoltaic effect, which is analogous to photodetectors based on dual-gated graphene **[17]** and WSe_2 P-N junctions **[18-21]**. However, the carrier density and carrier mobility in the n-doped region by the electrostatic gating of few layer black phosphorene is relatively low **[22, 23]**, which limits the built-in electrical potential and the separation efficiency of photogenerated carriers, thus limits the performance of phototransistors. In addition, the gate-induced stress effect in dual-gated FET devices on SiO_2 wafer reduces the performance and stability of the P-N junctions **[16]**.

Other strategies such as contact engineering and thickness engineering are promising to fabricate n-type BP FETs with high mobilities, however, are not capable of being integrated into P-N junctions **[24]**. In this regard, several theoretical works have alternatively been proposed to achieve n-doping of black phosphorene utilizing charge transfer from chemical dopants **[25]**. Notably, in comparison with conventional substitutional doping methods, the chemical doping can obtain a high carrier concentration while still maintain the high carrier mobility of BP as the processes do not induce defects in the crystal lattices. Up to date, however, only a few experimental works

have been carried out to investigate, control and modulate the electrical and optical properties of the single layer or few-layer black phosphorene by chemical modifications **[26, 27]**.

In this work, we incorporate n-type doping of few-layer black phosphorene using benzyl viologen (BV) as the surface charge transfer donor and achieve a P-N junction by protecting selective regions of the channel with Al_2O_3. A theoretical model is developed to analyze the chemical doping effects of BV and to achieve n-type few-layer black phosphorene. Formation of the P-N junctions is crucial in determining the photoresponse in our black phosphorene photodetectors as the photogenerated carriers can be separated by the built-in electrical field. Our devices display a high responsivity of up to ~180 mA/W in the near infrared range (1.47 μm) together with a response time of ~15 ms. As a demonstration example, we also realized few-layer black phosphorene solar cells based on the fabricated P-N junction structures, with remarkable power conversion efficiency of 0.75% under continuous white light illumination.

2. Results and discussion

2.1 N-type doping mechanism and design.

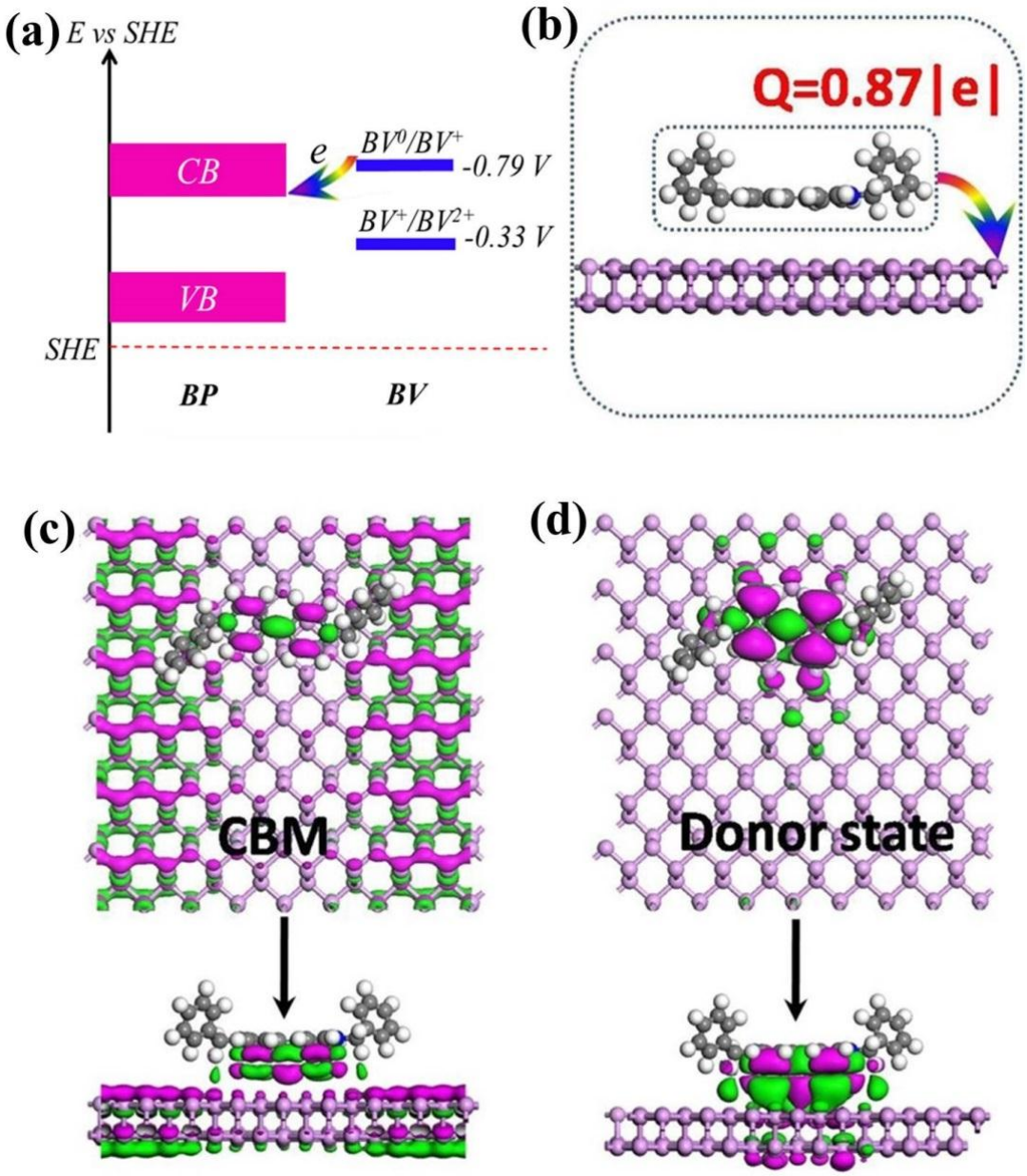

Figure 1 N-type chemical doping mechanism of black phosphorene. (a) Relative band alignment of BV molecule and phospherene corresponding to the standard hydrogen electrode (SHE). The energy level of BV molecule was reported in previous reports **[28]**. (b) The charge quantity transferred from a BV molecule to phospherene. We also mapped out the respective density profile of the electron at conduction band maximum (CBM) and donor state of BV doped monolayer phospherene. (c) Partial charge density of the conduction band minimum (CBM) and (d) the donor state of BV doped monolayer phospherene.

Molecule doping is a flexible and effective method towards modulating the electronic properties of 2D materials **[28-31]**. Here, we obtain n-type doing of few-layer black phosphorene by using a typical benzyl viologen (BV) for surface charge transfer. Based on the previously reported redox potentials for BV**[28]** (-0.79 V vs. SHE for BV^0/BV^+ and -0.30 V vs. SHE for BV^+/BV^{2+}, respectively) and the conduction band maximum (CBM) and valence band minimum (VBM) for bulk BP **[32]**, we can depict energy diagram of the few layer BP and BV as shown in Figure 1(a). Even though the VBM and CBM of few layer BP would be different from monolayer BP (the bandgap of few layer BP is narrower than that of monolayer BP), the BV reduction potentials are still at a higher energy level than the CBM of few layer BP. As a result, the Fermi level shifts to the conduction band minimum, and a flat band appears just below the Fermi level after doping with BV molecules. It is obvious that the flat bands may act as the donor states in the BV doped phosphorene system, as shown in Figures (b). In addition, to achieve a deeper insight into the electronic properties of the BV-doped phosphorene, we also mapped out the respective density profile of the electron at valence band maximum (VBM) and donor state of BV doped monolayer phospherene, as shown in Figure 1(c) and (d), respectively. The efficient electron transfer and shallow donor state suggest that the BV as an excellent donor doping in phosphorene system, can form a typical n-type semiconductor.

2.2 Few-layer BP P-N junction fabrication and characterization

In our experiments, reduced BV is synthesized and extracted by using a biphase of toluene and viologen-dissolved water **[30]** (Figure S2). The yield is confirmed by the absorption spectra where the peak intensity at ~405 nm was changed but no peak shift is

observed with various BV concentrations (Figure S3). Few-layer black phosphorene on a SiO_2 (285 nm)/Si substrate is peeled off via a modified mechanical exfoliation method and identified by optical microscopy and characterized by AFM (Figure S4) **[33]**. Black phosphorene FET is fabricated through standard e-beam evaporation after a photolithography process and the optical image of the device is shown in Figure S5. Note that few-layer black phosphorene is unstable in air and in water, we use a high concentration developer (>75%) and avoid the over-development of the photoresist. In order to obtain lateral P-N junction in the channel, we first cover half area of the black phosphorene with Al_2O_3 which is in-situ oxidized by placing the thermal evaporated 10 nm Al in O_2 ambient for 6 hours while the other part of the device is protected by photoresist. The AFM image (Figure S6) and XPS (Figure S7) demonstrate that uniform Al_2O_3 film is obtained by this simple strategy. Consequently, the photoresist is removed by acetone and kept in a vacuum chamber before further treatment. Lastly, the device is immersed in the BV solution (in toluene) and BV molecules are absorbed on the surface of the exposed area, forming a P-N junction while the Al_2O_3 covered region remains p-type as shown in Figure S8.

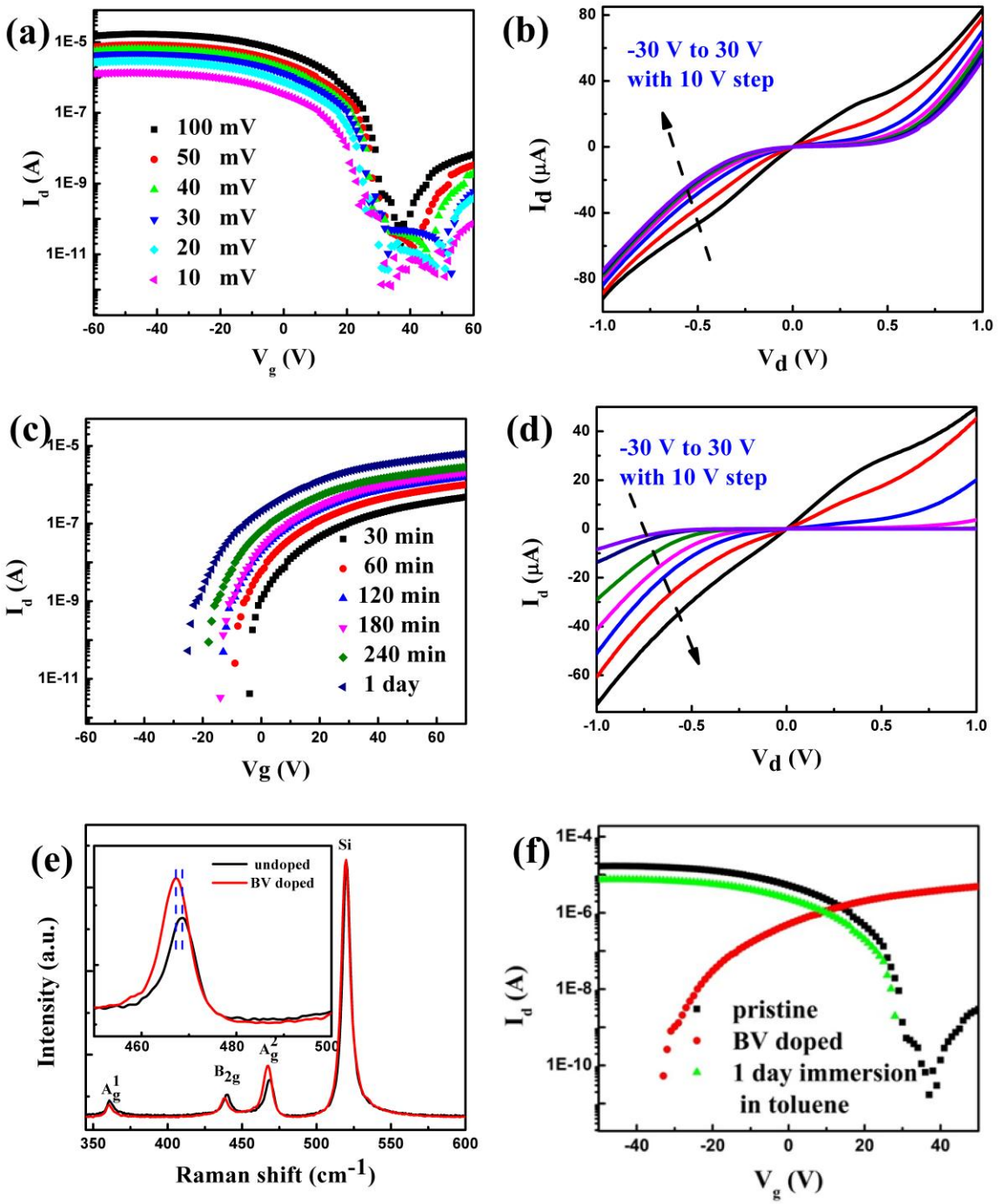

Figure 2 BV doping effect of few-layer black phosphorene. (a) Transfer characteristic curve of the source-drain current (I_d) versus gate voltage (V_g) of the BP FET recorded at the indicated source-drain voltages (V_d). (b) Source-drain current (I_d) versus source-drain voltage (V_d) of the BP FET recorded at different gate voltages (V_g) ranging from -30 V to 30 V with a step of 10 V. (c) Transfer characteristic curve of the source-drain current (I_d)

versus gate voltage (V_g) of the BV doped BP FET with different doping times. (d) Source-drain current (I_d) versus source-drain voltage (V_d) of the BV doped BP FET recorded at different gate voltages (V_g) ranging from -30 V to 30 V with a step of 10 V, the doping time for this measurement is 60 min. (e) Raman spectrum of the BP flake before (undoped, black curve) and after BV doping with 60 min (doped, red curve). (f) Reversibility of the BV doping effect of black phosphorus.

The few-layer BP flake of ~20 μm×1.4 μm is exfoliated from bulk BP crystal and transferred to a heavily doped silicon substrate with a 285 nm SiO_2 capping layer. The thickness of the flake is ~2.9 nm (5 layers), which is measured by atomic force microscopy (AFM) as shown in Figure S5. The Raman spectrum of the channel area of the BP FET is depicted in Figure 2(e). The peaks at ~361 cm^{-1}, ~440 cm^{-1}, ~468 cm^{-1} originate from the vibrations of the crystalline lattice, which is attributed to the A_g^1, B_g^2 and A_g^2 phonon modes and matched well with the Raman spectroscopy in bulk black phosphorus **[34]** and recent studies of single and few-layer phosphorene **[27, 35, 36]**. The I-V output of the few-layer BP FET shows a clear signature of p-type transistor behavior as shown in Figure 2(a) and 2(b). The drain current varies linearly with small source-drain biases, indicating a Schottky-like contact at the metal/BP interface. The mobility can be calculated by $\mu = \frac{L}{W \times (\varepsilon_0 \varepsilon_r / d)} \times \frac{dI_d}{dV_g} \times \frac{1}{V_d}$, where L=1.7 μm, W=1.4 μm and d=285 nm denote the channel length, width and the thickness of SiO_2 layer (285 nm in our experiments), respectively. V_d, I_d and V_b denote the source–drain bias, source–drain current, and bottom gate voltage in the linear region in the I_d–V_g curve. ε_0 and ε_r are the vacuum dielectric constant and the dielectric constant of SiO_2 (ε_r = 3.9), respectively. The calculated mobility of our device is about 180 cm^2/V s, which is on a par with the previous reports **[37-39]**. On the other hand, the hole concentration can be estimated

based on the transfer plot by the formula below: $n = -\frac{C_i(V_g - V_{th})}{e}$, where C_i is the capacitance per unit area between BP and the back gate is given by $C_i = \varepsilon_0\varepsilon_r / d$ and V_{th} is the threshold voltage of the device. For example, the electron concentration under V_g = 60 V bias can be estimated to be ~2.5×10^{12} cm^{-2}, which is much higher than those obtained by dual-gated BP P-N junctions [16] and WSe_2 P-N junctions **[21]**. This demonstrats the unique advantages of the chemical doping strategy proposed in this work.

After BV doping, the carrier type is converted from p-type (hole carrier) to n-type (electron carrier) as shown in Figure 2(c) and 2(d) that the BV doped BP FET exhibits high on-current as positive gate bias while negligible off-current at negative gate bias. The mobility of the FET is ~100 cm^2/V s for the device doped in BV solution for 240 min, which is about half of the pristine BP FET. However, the electron mobility of our devices is much higher than those obtained by the conventional electrostatic gating method **[16, 38]**, presenting a unique feature of BV based n-type doping method. To furher explore the mechanism to the doping strategy, the doped samples are also characterized by Raman spectroscopy (Figure 2(e)). Compared to pristine samples, the A_g^2 shifts to a lower wavenumber due to the softening of A_g^2 vibrations at high electron concentrations, indicating a Fermi level shift in the few-layer BP flake. Furthermore, the full width at half maximum (FWHM) of the A_g^2 peak shows a clear broadening, which is analogous to G-peak broadening in doped graphene **[40]**. All these indicate that the doping effect can be ascribed to the electron donation of BP during the charge state conversion of viologen from V^0 to V^{2+} as shown in Figure 1(d) and Figure S2. Another unique property of this method is that the BV molecule can be desorbed by immersing in toluene solution. The

dopant molecules gradually desorb from the surface and dissolve in toluene after immersion for 24 hours, and the doping effects are converted back to the original state as shown in Figure 2(f). The dependence of mobility on doping times and the reversibility of the doping effect indicate that the carrier type and concentration can be controllably engineered by the dopant amount and time, making it promising to fabricate N-type black phosphorne and further P-N junctions within the channel.

2.3 Electrical characterization of few-layer BP P-N junction

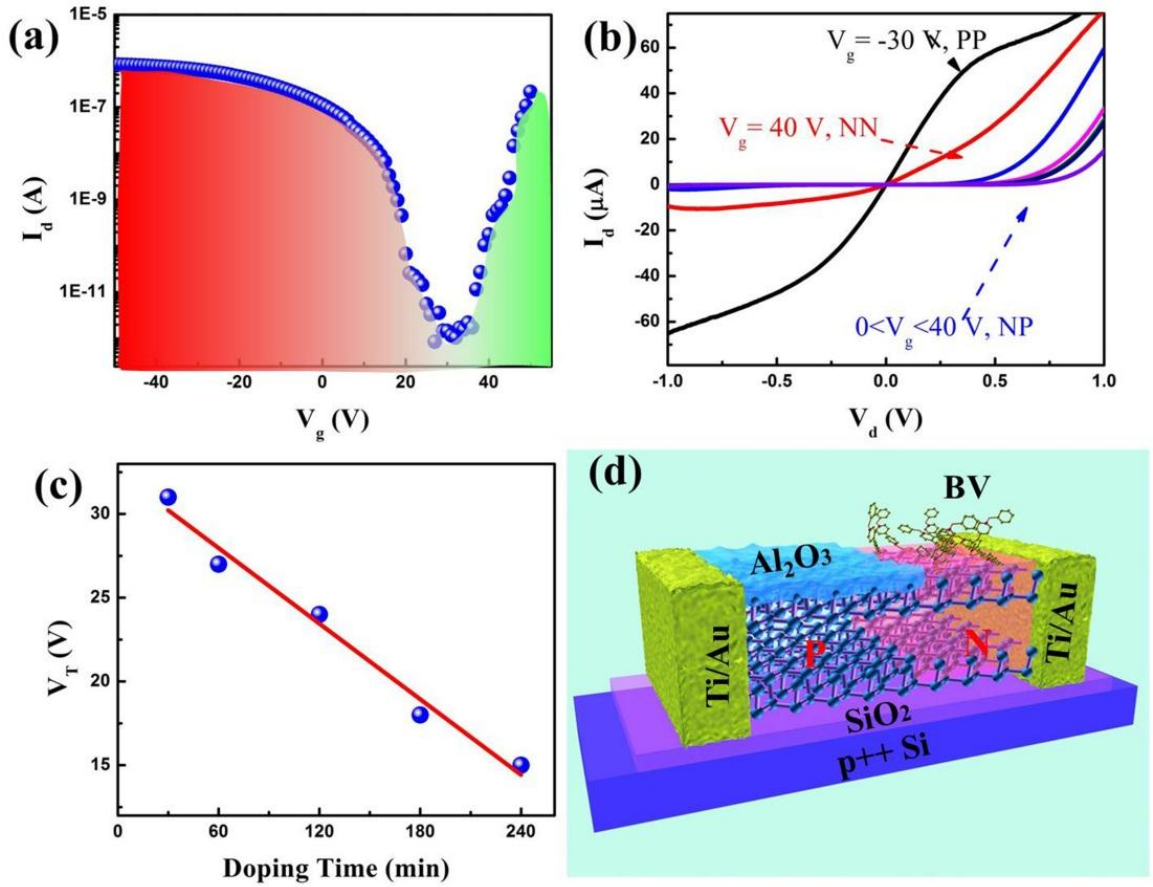

Figure 3 Electrical characterization of partially BV-doped BP P-N junction. (a) Transfer characteristic curve of the source-drain current (I_d) versus gate voltage (V_g) of the BP FET immersed in BV solution for 60 min. (b) Source-drain current (I_d) versus source-drain voltage (V_d) of the BV doped BP FET recorded at different gate voltages (V_g) ranging from -30 V to 30 V with a step of 10 V, the doping time is 60 min. (c)

Transfer voltage of the BV doped BP FET as a function of the doping time. (d) Band diagrams illustrating the different device configurations with various gate voltages.

Covering the BP channel partially can independently control the carrier type and density on the left and right side as shown in Figure 1(d). The partially doped BP FET shows low off-current down to 10^{-12} A and large on-current in both p-region and n-region (Figure 3(a)), indicating good control of the doping type and concentration in the BP channel. By varying the bottom gate, the channel can be converted from PP type to NN type. In Figure 3(b), device located in the NN ($V_g = -30$ V) and PP ($V_g = 40$ V) region exhibit much higher current values compared to those of NP region ($0 < V_g < 40$ V). On the other hand, the negligible current in the NP configuration with a reverse bias and the high rectification ($>10^5$) factor in the I-V characteristic indicate the formation of a junction diode. The origin of the strong current modulation induced by gating can be explained by the band diagram in Figure 3 (d). The PP and NN regions show higher current because the hole (or electron) conduction is dominant as the homogeneous electric field formed in the channel.

Figure 3(c) shows the controllability of the doping efficiency on the channel, which is essential in designing the mobility of various semiconductor devices. Analogous to other two dimensional materials, we define the voltage where the carrier changes from n-type (p-type) to p-type (p-type) with the transfer voltage (V_T). With an increasing doping time, V_T decreases from 31 V to 15 V, which is consistent with the results in BV doped BP FET as shown in Figure 3(c) and shows a higher doping level with longer doping time. Therefore, the transfer voltage of the formed P-N junction can be tuned flexibly by controlling the doping time. By fitting the I-V curve of the p-n junction in Figure 3(b) with a modified Schottky diode equation based on Lambert W-function **[41]**

(see Supplementary Information) and extended to include a series resistance (R_S): $I_d = \frac{nV_t}{R_S} W\left\{\frac{I_S R_S}{nV_t}\exp\left(\frac{(V_d + I_S R_S)}{nV_t}\right)\right\} - I_0$, where n is the diode ideality factor (n=1 is the ideal case), W is the Lambert W function. We also obtain n = 2.28~2.63 for the devices operating in the P-N configuration, which is higher than that of the dual-gated WSe_2 P-N junctions.[20, 21] The high ideal factor might be attributed to high defect scatterings induced by chemical doping processes and also indicates that the source-drain current is mainly limited by the recombination rather than diffusion **[42]**. On the other hand, we obtain R_S~2 MΩ due to the contact resistance at the BP/electrode interface. The series resistance (R_S) is one order smaller than the dual-gated BP or WSe_2 P-N junctions **[16, 21]**, and also smaller than WSe_2 P-N junctions capped with a high-k HfO_2 layer**[20]**. This demonstrates another advantage of our strategy of chemically doped P-N junction. Our observation also agrees well with the previous report that the contact resistance can be reduced by ~3 times through BV doping of MoS_2 **[28]**. Another effect that contributes to the small R_s is the passivated Al_2O_3 layer which decreases the contact barrier of the BP/ Al_2O_3 interface. As reported before, the negative fixed charges originated from the Al_2O_3 layer induces band bending in the BP/ Al_2O_3 interface **[43]**. The in-situ oxidized amorphous Al_2O_3 layer may induce negative fixed charges by the following two mechanisms. Firstly, the Al_2O_3 layer could be dissociated into negative $AlO_{4/2}^-$ structures compensated by positive Al^{3+}. Secondly, the OH groups as indicated in the XPS spectrum (Figure S7) would be trapped in the Al_2O_3 layer. Investigating the effects of chemical doping and a passivation layer on the contact resistance and FET device performance will be the focus of future works.

2.4 Optoelectronic properties of few-layer BP P-N junction

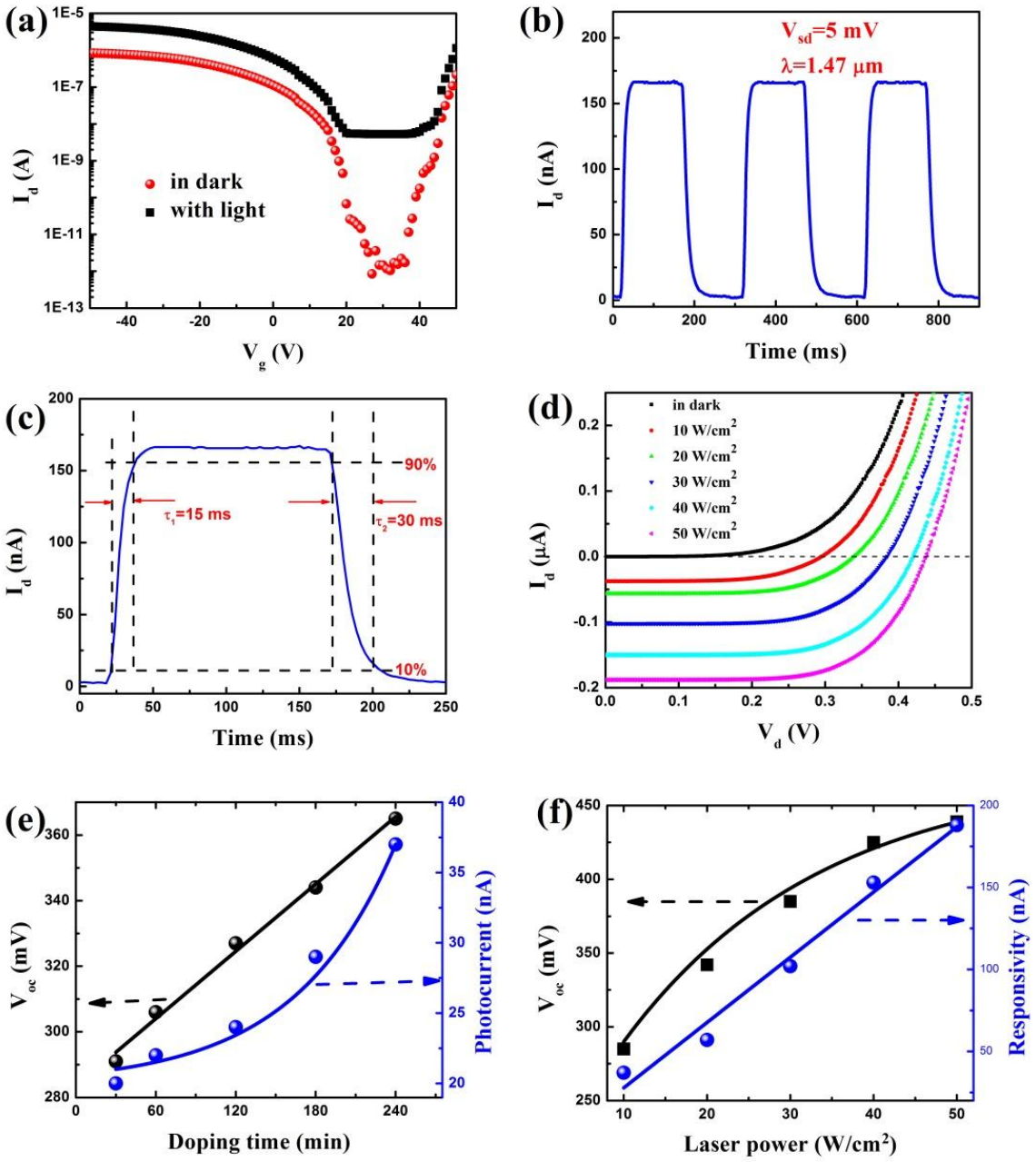

Figure 4 Optoelectronic performance of BV-doped BP P-N junction. (a) Gating response (I_d-V_g) of BP P-N junction photodetector in dark (red dots) and under 1.47 μm fiber laser illumination (black dots), acquired for backgate voltage V_g between -50 V to 50 V. Illumination power density is 50 W/cm^2. (b) Time-resolved photocurrent under modulated laser excitation (~5 Hz, P=50 W/cm^2), recorded for bias voltage V_d = 5mV and gate voltage Vg = 30 V. The sample measured in (a) and (b) are the same sample which is doped for 30 min. (c) Zoom on a single switching cycle at 5Hz frequency. Rise

(fall) times are defined as the time for current rising from 10% to 90% (90% to 10%) of the maximum photocurrent. (d) I-V characteristics in P-N configuration under illumination with different power densities (10 to 50 W/cm^2) on the device. The intersections of the I-V curve with the coordinates are defined as open-circuit voltage V_{oc} (X-axis) and short-circuit current I_{sc} (Y-axis). (e) Dependence of open-circuit voltage (V_{oc}) and photocurrent on doping time, recorded for bias voltage at V_d = 5mV and illumination power density of 10 W/cm^2. (f) Dependence of open-circuit voltage (V_{oc}) and photocurrent on illumination density. The sample is doped for 30 min.

The efficient and tunable P-N junction is critical to the separation of photoexcited electron/hole pairs and thus allows us to investigate the properties of optoelectronic devices such as photodetector and solar cell based on BP P-N junction diodes. The whole device is illuminated by a laser beam (λ = 1.47 μm) with a diameter of ~500 μm. The photocurrent dependence on backgate voltage as shown in figure 4(a) clearly indicates that the off-current increases ~4 orders, demonstrating that the photocurrent dominates over thermionic and tunneling currents in the photodiode operation with backgate voltage ranging from −50 V to 50 V. In Figure 4(b) and (c), we explore the time-resolved photo-switching by a modulated laser beam (λ = 1.47 μm) via a mechanical chopper with a frequency of 5 Hz (see Supplementary Information). This demonstrates that BP based devices are can be operated in the near-infrared range, which is superior to other 2D materials based photodetectors limited in the visible or ultraviolet range due to their larger bandgap **[6, 7, 21, 44]**. The responsivity (R) is obtained by $R = I_{ph} / P_{in}$, where the photocurrent $I_{ph} = I_{on} - I_{off}$ and P_{in} is the input power incident on the device area. We measure responsivity up to 180 mA/W under power density of 50 W/cm^2 with a small source-drain bias (V_d = 5 mV), and find that the responsivity increases with the decrease of excitation laser power density (Figure 4f). By fitting the responsivity vs power density

with $R = CP_d^{\alpha-1}$ (C is constant) we get α = 0.82, indicating that the high recombination of the photogenerated carriers is attributed to the trap states and electron/phonon interactions **[45]**. In our experiments, the recombination efficiency can be greatly reduced by the built-in electric field (P-N junction barrier). As a result, the photocurrent, under a constant illumination, increases exponentially with the increasing of doping time which controls the doping level and thus tunes the formed built-in electric field.

The response time (τ) and detectivity (D) of the photodetector are other key specifications for the BP P-N junction photodetector. As shown in Figure 4(c), we measure the 10%-90% rise and fall times are τ_1 = 15 ms and τ_2 = 30 ms, respectively. The response times are on a par with previous BP based photodetectors and can be further enhanced by optimizing the doping process and the device architectures. The slower fall time observed in our experiment might be related to the relaxation of deeply trapped states. From the practical point of view, specific detectivity is a measure of detector sensitivity and given by $D = I_{ph} / P_d \sqrt{2eI_{dark}}$, where I_{dark} is the dark current generated by the thermionic and tunneling effect. The detectivity for our devices under 1.47 μm is in the range of 10^{11}-10^{13} cm $Hz^{1/2}$/W and increases with the increasing of doping time, which could be explained by the fact that longer doping time forms the higher barrier that blocks the thermionic and tunneling current. The detectivity of the BP P-N junction photodetectors is on a par with common near infrared photodetectors based on Si, InGaAs and polymer having a detectivity of ~10^{12}~10^{13} cm $Hz^{1/2}$/W, which is limited by shot noise of the dark current **[46]**.

We now turn to the specifications of the power conversion properties of the BP P-N junction. Figure 4(d) displays I-V characteristics in P-N configuration under

illumination (λ=1.47 μm) with various power densities. The open-circuit voltage (V_{OC}) which is determined by the barrier height shows a linear dependence on the doping time and thus could be tuned by the BV doping as shown in Figure 4(e). Furthermore, the open-circuit voltage (V_{OC}) increasing logarithmically and short-circuit current (I_{SC}) increasing linearly with the increase of power density as shown in Figure 4(f) are in good agreement with ideal solar cell configuration, demonstrating the photocurrent generation is dominated by the photovoltaic effect **[21]**.

To investigate the power conversion efficiency (η) of the fabricated BP P-N junction diode as a solar cell, we consider the active area to be the entire BP channel region between the source and drain electrodes as an estimate. According to the configuration of a conventional solar cell, the output electric power can be calculated by $P_{out} = V_{OC} \times I_{SC} \times FF$, where FF is the filling factor and determined by the ratio of the area covered by the I-V curve to the maximum output power $P_{\max} = V_{OC} \times I_{SC}$, and can be defined as $FF = \int_0^{V_{OC}} I(V) d_V / (V_{OC} \times I_{SC})$. The power conversion efficiency (η) is defined as $\eta = P_{out} / P_{in}$. For instance, we obtain η~0.75% for the input power density of 10 W/cm^2, which is higher than previous reports even though it is underestimated as we assume the whole channel is the active region rather than the depletion region only **[16]**.

3. Conclusion

In summary, we have demonstrated that few-layer BP P-N junction phototransistors fabricated by partially BV doping show strong rectifying current. The barrier height of the P-N junction can be controlled by the doping time and efficiently separate the photogenerated electron/hole pairs. Under near infrared laser illumination on the junction, the diodes produce considerable performance with high detectivity of ~10^{11}-

10^{13} Jones and responsivity of ~180 mA/W at a low bias of 5 mV via photovoltaic effect. Furthermore, we have also demonstrated that the fabricated BP P-N junction diode can be employed as a photovoltaic solar cell with power energy conversion efficiency of ~0.75%. Our results are expected to fabricate flexible and transparent photodetectors and solar cells that could be compatible with glass and polymer substrates, promising for new generations of high performance charge-coupled devices (CCD), image sensors, displays and solar cells. We also expect our environmental encapsulation techniques to be applicable to the research of other two-dimensional materials.

Supporting Information

Supplementary data associated with this article can be found in the online version.

Acknowledgements

This work was supported by MOE2011-T2-2-147 from Ministry of Education, Singapore. SZ and HZ would like to thank the funding support from national Basic Research Program of China (grant number 2014CB931700), NSFC (grant number 61222403) and the Priority Academic Program Development of Jiangsu Higher Education Institutions. X. Y. and S. Z. contribute equally to this work.

References

[1] Fiori, G.; Bonaccorso, F.; Iannaccone, G.; Palacios, T.; Neumaier, D.; Seabaugh, A.; Banerjee, S. K.; Colombo, L. *Nat. Nanotechol.* 9 (2014) 768-779.
[2] Li, J.; Niu, L.; Zheng, Z.; Yan, F. *Adv. Mater.* 26 (2014) 5239-5273.
[3] Koppens, F. H. L.; Mueller, T.; Avouris, P.; Ferrari, A. C.; Vitiello, M. S.; Polini, M. *Nat. Nanotechol.* 9 (2014) 780-793.
[4] Sun, Z.; Chang, H. *ACS Nano* 8 (2014) 4133-4256.
[5] RadisavljevicB; RadenovicA; BrivioJ; GiacomettiV; KisA. *Nat. Nanotechol.* 6 (2011) 147-150.
[6] Choi, W.; Cho, M. Y.; Konar, A.; Lee, J. H.; Cha, G.-B.; Hong, S. C.; Kim, S.; Kim, J.; Jena, D.; Joo, J.; Kim, S. *Adv. Mater.* 24 (2012) 5832-5836.
[7] Lopez-Sanchez, O.; Lembke, D.; Kayci, M.; Radenovic, A.; Kis, A. *Nat. Nanotechol.* 8 (2013) 497-501.
[8] Tran, V.; Soklaski, R.; Liang, Y.; Yang, L. *Phys. Rev. B* 89 (2014) 235319.
[9] Kou, L.; Chen, C.; Smith, S. C. *J. Phys. Chem. Lett.* 6 (2015) 2794-2805.
[10] Qiao, J.; Kong, X.; Hu, Z.-X.; Yang, F.; Ji, W. *Nat. Commun.* 5 (2014) 4475.
[11] Xia, F.; Wang, H.; Xiao, D.; Dubey, M.; Ramasubramaniam, A. *Nat. Photonics* 8 (2014) 899-907.

[12] Li, L.; Ye, G. J.; Tran, V.; Fei, R.; Chen, G.; Wang, H.; Wang, J.; Watanabe, K.; Taniguchi, T.; Yang, L.; Chen, X. H.; Zhang, Y. *Nat. Nanotechol.* 10 (2015) 608-613.
[13] Youngblood, N.; Chen, C.; Koester, S. J.; Li, M. *Nat. Photon.* 9 (2015) 247-252.
[14] Engel, M.; Steiner, M.; Avouris, P. *Nano Lett.* 14 (2014) 6414-6417.
[15] Buscema, M.; Groenendijk, D. J.; Blanter, S. I.; Steele, G. A.; van der Zant, H. S. J.; Castellanos-Gomez, A. *Nano Lett.* 14 (2014) 3347-3352.
[16] Buscema, M.; Groenendijk, D. J.; Steele, G. A.; van der Zant, H. S. J.; Castellanos-Gomez, A. *Nat. Commun.* 5 (2014) 4651.
[17] Gabor, N. M.; Song, J. C. W.; Ma, Q.; Nair, N. L.; Taychatanapat, T.; Watanabe, K.; Taniguchi, T.; Levitov, L. S.; Jarillo-Herrero, P. *Science* 334 (2011) 648-652.
[18] Ross, J. S.; Klement, P.; Jones, A. M.; Ghimire, N. J.; Yan, J.; Mandrus, D. G.; Taniguchi, T.; Watanabe, K.; Kitamura, K.; Yao, W.; Cobden, D. H.; Xu, X. *Nat. Nanotechol.* 9 (2014) 268-272.
[19] Pospischil, A.; Furchi, M. M.; Mueller, T. *Nat. Nanotechol.* 9 (2014) 257-261.
[20] Baugher, B. W. H.; Churchill, H. O. H.; Yang, Y. F.; Jarillo-Herrero, P. *Nat. Nanotechnol.* 9 (2014) 262-267.
[21] Groenendijk, D. J.; Buscema, M.; Steele, G. A.; Michaelis de Vasconcellos, S.; Bratschitsch, R.; van der Zant, H. S. J.; Castellanos-Gomez, A. *Nano Lett.* 14 (2014) 5846-5852.
[22] Du, Y.; Liu, H.; Deng, Y.; Ye, P. D. *ACS Nano* 8 (2014) 10035-10042.
[23] Xia, F.; Wang, H.; Jia, Y. *Nat. Commun.* 5 (2014) 4458.
[24] Perello, D. J.; Chae, S. H.; Song, S.; Lee, Y. H. *Nat. Commun.* 6 (2015).
[25] Rudenko, A. N.; Katsnelson, M. I. *Phys. Rev. B* 89 (2014) 201408.
[26] Kim, J.; Baik, S. S.; Ryu, S. H.; Sohn, Y.; Park, S.; Park, B.-G.; Denlinger, J.; Yi, Y.; Choi, H. J.; Kim, K. S. *Science* 349 (2015) 723-726.
[27] Ziletti, A.; Carvalho, A.; Trevisanutto, P. E.; Campbell, D. K.; Coker, D. F.; Castro Neto, A. H. *Phys. Rev. B* 91 (2015) 085407.
[28] Kiriya, D.; Tosun, M.; Zhao, P.; Kang, J. S.; Javey, A. *J. Am. Chem. Soc.* 136 (2014) 7853-7856.
[29] Liu, Y.; Xu, F.; Zhang, Z.; Penev, E. S.; Yakobson, B. I. *Nano Lett.* 14 (2014) 6782-6786.
[30] Kim, S. M.; Jang, J. H.; Kim, K. K.; Park, H. K.; Bae, J. J.; Yu, W. J.; Lee, I. H.; Kim, G.; Loc, D. D.; Kim, U. J.; Lee, E.-H.; Shin, H.-J.; Choi, J.-Y.; Lee, Y. H. *J. Am. Chem. Soc.* 131 (2009) 327-331.
[31] Yu, Z.; Pan, Y.; Shen, Y.; Wang, Z.; Ong, Z.-Y.; Xu, T.; Xin, R.; Pan, L.; Wang, B.; Sun, L.; Wang, J.; Zhang, G.; Zhang, Y. W.; Shi, Y.; Wang, X. *Nat. Commun.* 5 (2014) 5290.
[32] Takahashi, T.; Shirotani, K.; Suzuki, S.; Sagawa, T. *Solid State Communications* 45 (1983) 945-948.
[33] Andres, C.-G.; Leonardo, V.; Elsa, P.; Joshua, O. I.; Narasimha-Acharya, K. L.; Sofya, I. B.; Dirk, J. G.; Michele, B.; Gary, A. S.; Alvarez, J. V.; Henny, W. Z.; Palacios, J. J.; Herre, S. J. v. d. Z. *2D Mater.* 1 (2014) 025001.
[34] Sugai, S.; Shirotani, I. *Solid State Commun.* 53 (1985) 753-755.
[35] Zhang, S.; Yang, J.; Xu, R.; Wang, F.; Li, W.; Ghufran, M.; Zhang, Y.-W.; Yu, Z.; Zhang, G.; Qin, Q.; Lu, Y. *ACS Nano* 8 (2014) 9590-9596.

[36] Liu, H.; Neal, A. T.; Zhu, Z.; Luo, Z.; Xu, X.; Tománek, D.; Ye, P. D. *ACS Nano* 8 (2014) 4033-4041.
[37] Li, L.; Yu, Y.; Ye, G. J.; Ge, Q.; Ou, X.; Wu, H.; Feng, D.; Chen, X. H.; Zhang, Y. *Nat. Nanotechnol.* 9 (2014) 372-377.
[38] Das, S.; Demarteau, M.; Roelofs, A. K. *ACS Nano* 8 (2014) 11730-11738.
[39] Xiang, D.; Han, C.; Wu, J.; Zhong, S.; Liu, Y.; Lin, J.; Zhang, X.-A.; Ping Hu, W.; Özyilmaz, B.; Neto, A. H. C.; Wee, A. T. S.; Chen, W. *Nat. Commun.* 6 (2015) 6485.
[40] Das, A.; Pisana, S.; Chakraborty, B.; Piscanec, S.; Saha, S. K.; Waghmare, U. V.; Novoselov, K. S.; Krishnamurthy, H. R.; Geim, A. K.; Ferrari, A. C.; Sood, A. K. *Nat. Nanotechol.* 3 (2008) 210-215.
[41] Ortiz-Conde, A.; García Sánchez, F. J.; Muci, J. *Solid-State Electron.* 44 (2000) 1861-1864.
[42] Banwell, T. C.; Jayakumar, A. *Electron. Lett.* 36 (2000) 291-292.
[43] Han, L.; Neal, A. T.; Mengwei, S.; Yuchen, D.; Ye, P. D. *IEEE, Electron Device Lett.* 35 (2014) 795-797.
[44] Li, H.; Shi, Y.; Chiu, M.-H.; Li, L.-J. *Nano Energy* 18 (2015) 293-305.
[45] Yu, X.; Shen, Y.; Liu, T.; Wu, T.; Wang, Q. *Sci. Rep.* 5 (2015) 12014.
[46] Gong, X.; Tong, M.; Xia, Y.; Cai, W.; Moon, J. S.; Cao, Y.; Yu, G.; Shieh, C.-L.; Nilsson, B.; Heeger, A. J. *Science* 325 (2009) 1665-1667.

Xuechao Yu received his Master degree in material physics and chemistry from Chinese Academic of Sciences in 2012 and he entered School of EEE, Nanyang Technological University, Singapore, as a Ph.D. student in 2013. He is now working in Nanyang Technological Unversity as a research associate working on the photonic and optoelectronic applications of novel 2D materials.

Dr. Shengli Zhang received his Ph. D. from Beijing University of Chemical Technology in 2013. Then Dr. Zhang joined the Institute of Optoelectronics & Nanomaterials, Nanjing University of Science & Technology, His research interests include the electronic structure and optoelectronic properties of atomic layer materials and first principle calculations for novel 2D materials.

Prof. Haibo Zeng received his PhD from Institute of Solid State Physics, Chinese Academy of Sciences in 2006. Haibo later worked with Professor Claus Klingshirn in 2007 at University of Karlsruhe, Germany, lasting research on ZnO optics. In 2008, he joined Professor Yoshio Bando's group at National Institute for Materials Science (NIMS), Japan. In 2013, he moved to Nanjing University of Science and Technology as a distinguished professor and the director of Institute of Optoelectronics & Nanomaterials. His current research interest is low-dimensional semiconductor optoelectronics, including 2D materials and QDs. So far, he has published over 150 scientific papers with citation more than 6,000 times.

Prof. Qi Jie Wang received the B.E. degree from the University of Science and Technology of China (USTC) in 2001; and the Ph.D degree from Nanyang Technological University, Singapore, in 2005. Then he joined in Prof. Federico Capasso's group in Harvard University as a postdoctoral researcher in 2007. In 2009, he was assigned as a joint Nanyang Assistant Professor at EEE and SPMS. Since 2015, he has been promoted to tenured Associate Professor

in school of EEE, NTU. His current research interests are to explore theoretically and experimentally nano-structured semiconductor and nanophotonic devices.

Supporting Information

Lateral Black Phosphorene P-N Junctions Formed via Chemical Doping for High Performance Near-infrared Photodetector

Xuechao Yu[a], Shengli Zhang[b], Haibo Zeng[b,*], and Qi Jie Wang[a,*]

[a] Centre for OptoElectronics and Biophotonics, School of Electrical and Electronic Engineering, Nanyang Technological University, 50 Nanyang Avenue, 639798, Singapore

[b] Country Institute of Optoelectronics & Nanomaterials, Herbert Gleiter Institute of Nanoscience, College of Materials Science and Engineering, Nanjing University of Science and Technology, Nanjing, 210094, China

Computational methods

The computations were performed by using the DMol[3] code with all-electron method, under periodic boundary. Geometry optimization and band structure calculations were under the exchange correlation term of generalized gradient approximation (GGA)[1]. The double numerical plus polarization (DNP) basis set[2, 3] and Perdew, Burke, and Ernzerholf (PBE) functional[4] were adopted in all computations. It is known that the framework of standard PBE functional don't contain weak interactions, so PBE+D2 (D stands for dispersion) method with the Grimme vdW correction was adopted to describe the weak interactions[5]. To ensure high quality results, convergence criterion on the total energy and electronic computations was chosen as high as 10^{-6} a.u. and the real-space global orbital cutoff radius was 4.7 Å in all the self-consistent field (SCF) computations. To study TTF and BV doping of phosphorene, we adopt an 8×6×1 supercell with a large vacuum gap of 25 Å in the z direction. The Brillouin zone was sampled with a 3×3×1 Γ□centered *k* points setting in geometry optimization.

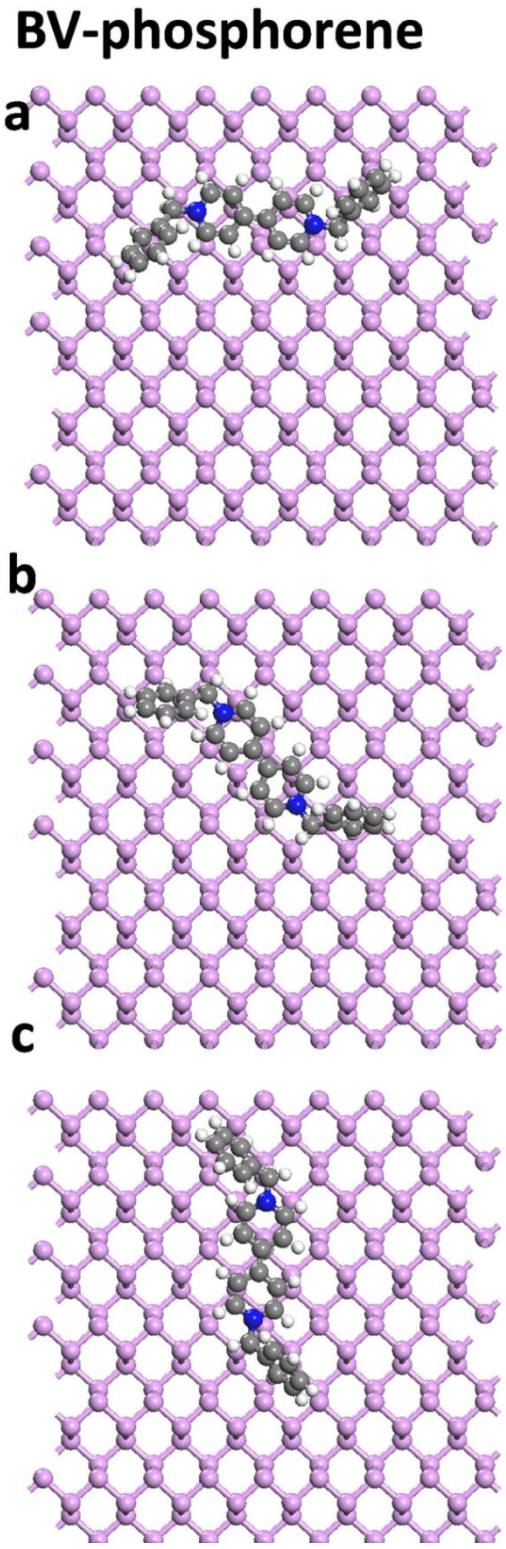

Figure S1. The optimized possible configurations for the adsorption of BV molecule on the basal plane of phosphorene.

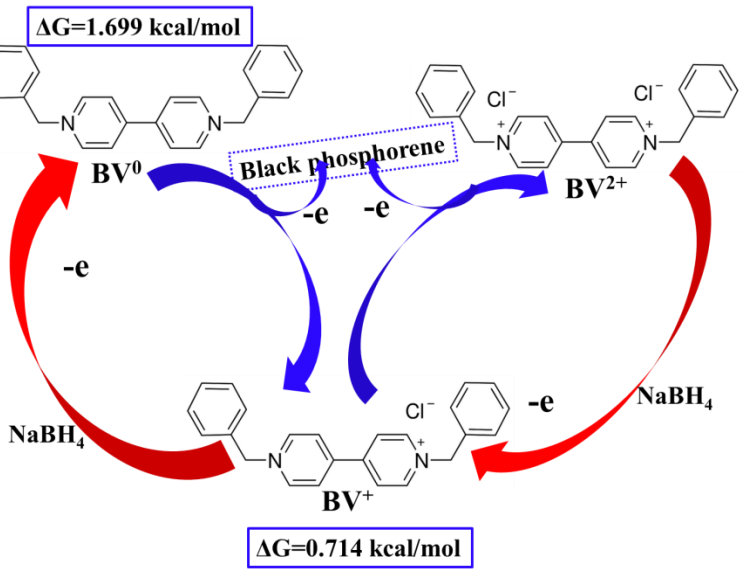

Figure S2. Reversible redox reactions of BV with Gibbs free energy differences.

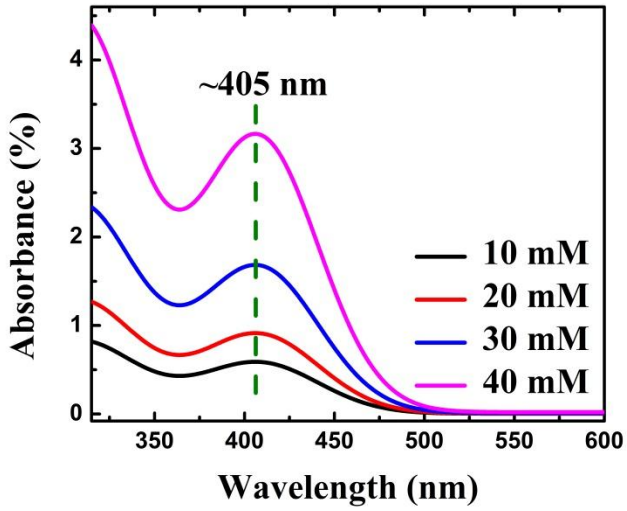

Figure S3. Absorption of the synthesized BV with various concentrations.

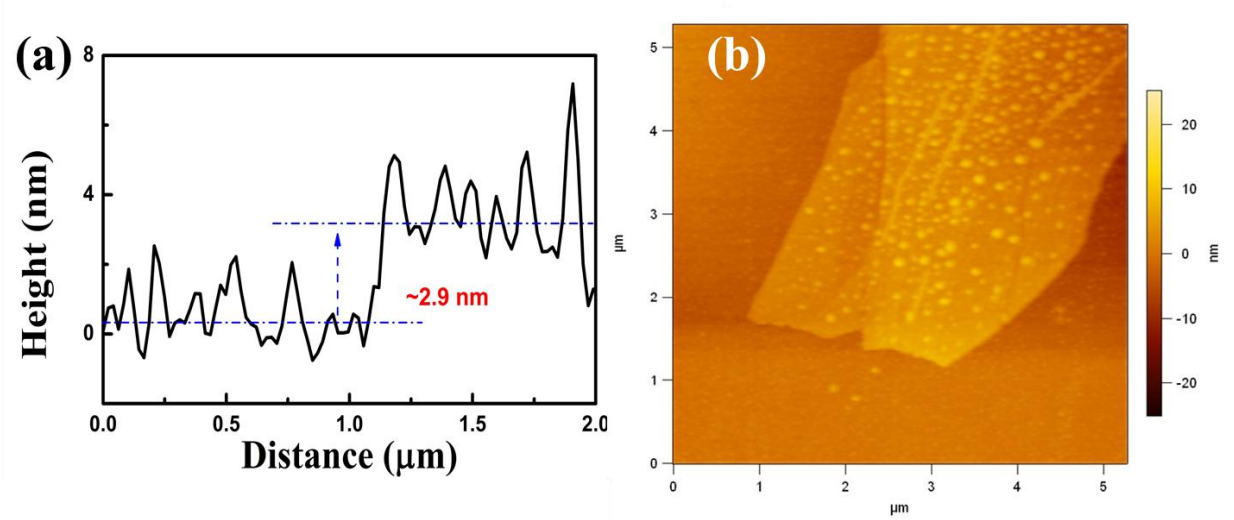

Figure S4. AFM height profile and image of few-layer black phosphorene.

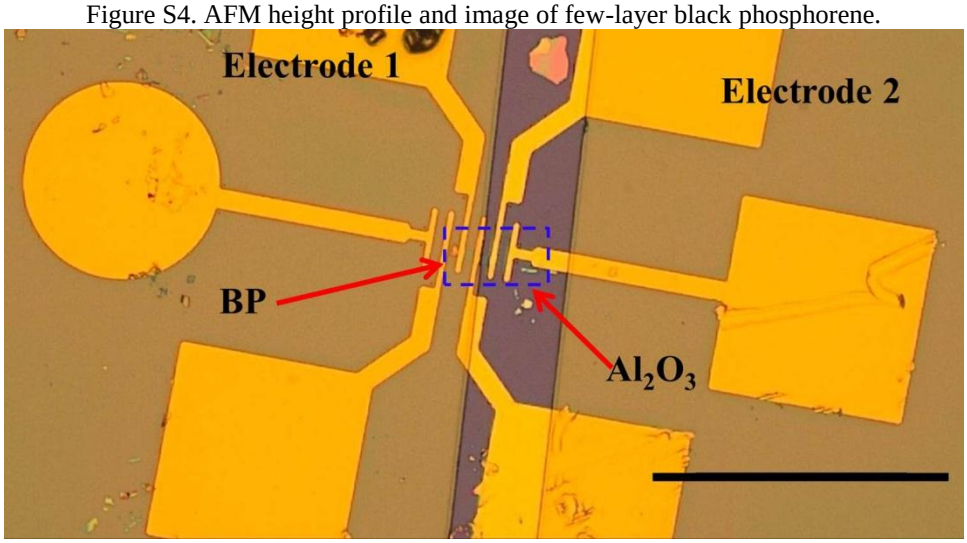

Figure S5. Optical image of few-layer BP p-n junction device. The scale bar is 100 μm.

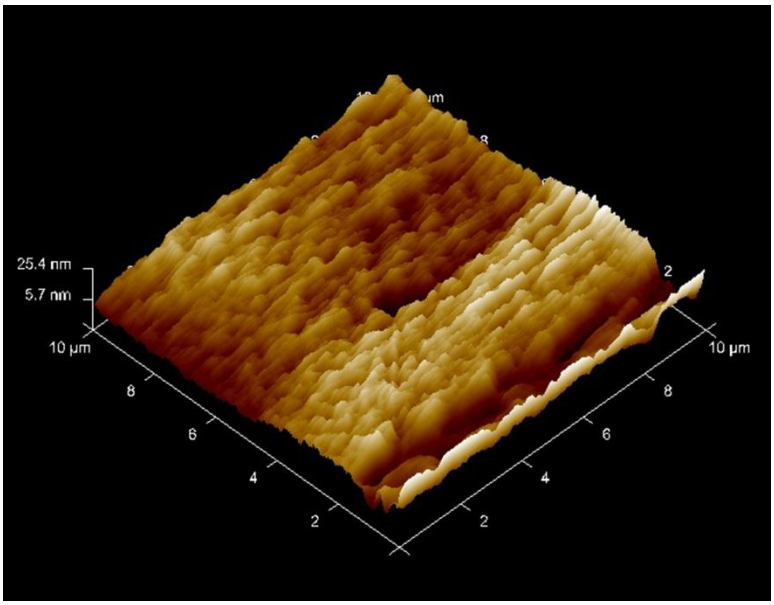

Figure S6. AFM image of in-situ oxidized Al_2O_3.

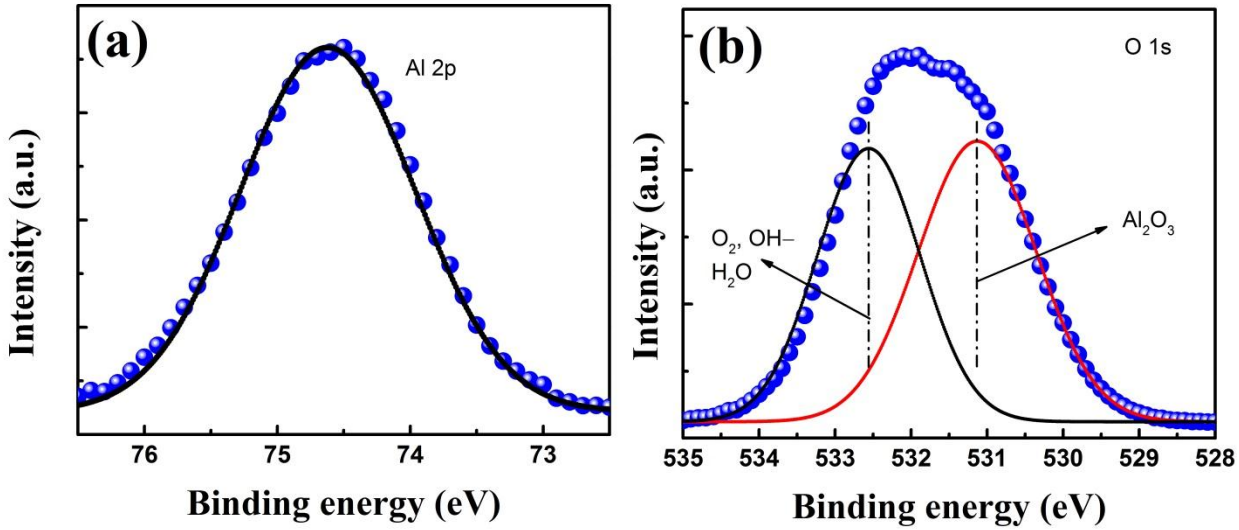

Figure S7. XPS spectrum of in-situ oxidized Al_2O_3. (a) Al 2p core level. (b) O 1s core level.

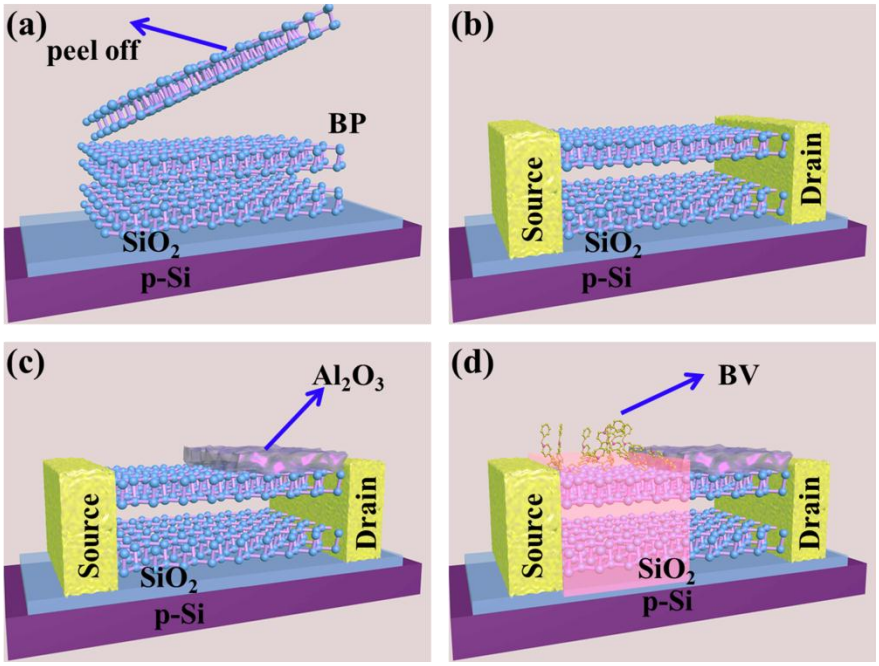

Figure S8. Schematic illustration of fabricating BV doping of few layer black phosphorene into P-N junction. (a) Few layer black phosphorene is isolated on SiO_2/Si wafer, the thickness of SiO_2 is 285 nm, heavily p-doped Si is also used as the bottom gate electrode. (b) Ti/Au (20 nm/80 nm) electrode is deposited by e-Beam evaporator after a photolithography process. (c) Half of the black phosphorene channel is covered by thermal evaporated Al which is oxidized into Al_2O_3 under ambient. (d) The Al_2O_3 covered black phosphorene field effect transistor (FET) is immersed in BV solution, the exposed area is n-doped by the BV molecule.

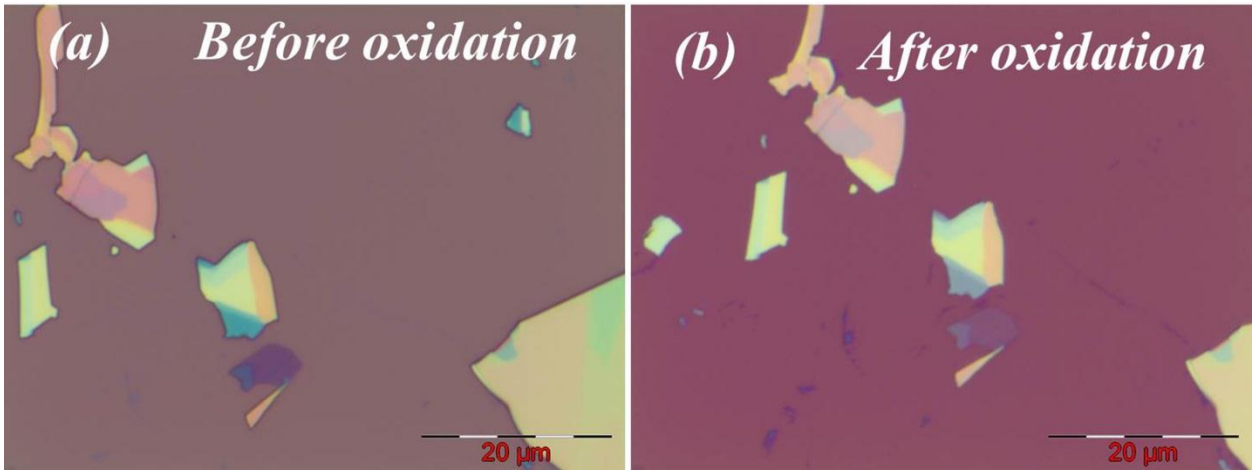

Figure S9. Optical images of few layer BP before (a) and after oxidation (b).

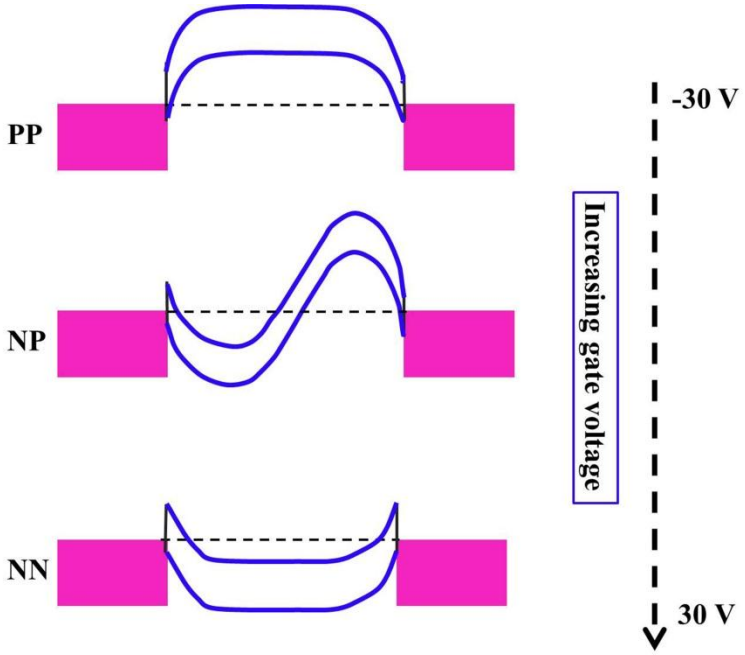

Figure S10. Energy band diagram of the formed black phosphorene P-N junction.

Device analysis:

The barrier height can be estimated by fitting the rectifying I-V curves with the modified Shockley equation

$$I_d = I_s \cdot [\exp(\frac{V_d - I_d R_S}{nV_t}) - 1] + \frac{V_d - I_d R_S}{R_P} + \frac{V}{R_{P2}} + \frac{VR_S}{R_{P1}R_{P2}}$$

$$I_d = \frac{nV_t}{R_S} W\left\{\frac{I_S R_S}{nV_t}\exp\left(\frac{(V_d + I_S R_S)}{nV_t}\right)\right\} - I_0$$

With $V_t = k_B T / q$

In the calculation of responsivity (R), $P_{in} = P_{density} \times S$. For example, when $P_{density}$ = 50 W/cm^2, Pin=0.9 μW. so we can estimated the R~180 mA/W.

References

1. Delley, B. *J. Chem. Phys.* **1990**, 92, 508-517.
2. Danov, K. D.; Petsev, D. N.; Denkov, N. D.; Borwankar, R. *J. Chem. Phys.* **1994**, 100, 6104-6104.
3. Delley, B. *J. Chem. Phys.* **2000**, 113, 7756-7764.
4. Perdew, J. P.; Burke, K.; Ernzerhof, M. *Phys. Rev. Lett.* **1996**, 77, 3865-3868.
5. Grimme, S. Semiempirical. *J. Comput. Chem.* **2006**, 27, 1787-1799.